

Thermal decay of two-spinon bound states in quasi-2D triangular antiferromagnets

I. L. Pomponio¹, E. A. Ghioldi², C. J. Gazza¹, L. O. Manuel¹, and A. E. Trumper¹

¹ *Instituto de Física Rosario (CONICET) and Facultad de Ciencias Exactas,*

Ingeniería y Agrimensura, Universidad Nacional de Rosario, 2000 Rosario, Argentina and

² *Department of Physics and Astronomy, University of Tennessee, Knoxville, Tennessee 37996-1200, USA*

We analyze the temperature evolution of the anomalous magnetic spectrum of the spin-1/2 triangular quantum Heisenberg antiferromagnet, which is proximate to a quantum critical point. Recently, its low energy excitations have been identified with two-spinon bound states, well defined in an ample region of the Brillouin zone. In this work, we compute the thermal magnetic spectrum within a Schwinger boson approach, incorporating Gaussian fluctuations around the saddle-point approximation. In order to account for a finite Néel temperature T_N , we incorporate an exchange interaction between triangular layers. As temperature rises, the dispersion relation of the two-spinon bound states, representing single-magnon excitations, remains unchanged but becomes mixed with the thermally activated spinon continuum. Consequently, a crossover occurs at a temperature $T^* \simeq 0.75T_N$, defining a *terminated Goldstone regime* between T^* and T_N , where only the Goldstone modes survives as well-defined magnon excitations, up to the Néel temperature. Our results support the idea that the fractionalization of magnons near a quantum critical point can be extended to more realistic quasi-2D frustrated antiferromagnets.

I. INTRODUCTION

The understanding of the organizing principles [1] governing frustrated antiferromagnets (AF) remains a debated topic in condensed matter physics [2]. The pursuit of quantum spin liquids —highly entangled quantum states without classical analogs and characterized by fractional spinon excitations— has been a central focus since the proposal of the resonant valence bond state for the triangular antiferromagnet [3–9]. This quest has driven both theoretical and experimental efforts, fueled by insights from high-temperature superconductors [10] and concepts from the fractional quantum Hall effect [11]. Advancements in numerical and analytical techniques, applied to a variety of frustrated models, have played a relevant role in validating zero-temperature quantum phase diagrams along with their corresponding low-lying magnetic excitations [12]. Additionally, the synthesis of new compounds [13] and the refinement of experimental techniques, such as inelastic neutron scattering (INS) [14], have confirmed the experimental realization of predicted exotic magnetic states of matter. In the current era of quantum materials [15, 16], it is crucial to integrate this knowledge to enable theoretical predictions of experiments under diverse conditions in an even more controlled manner.

In recent years, the synthesis of triangular antiferromagnets has notably increased, giving rise to numerous candidates for spin liquids [17, 18]. However, only few of them are perfectly equilateral, disordered-free, or faithfully realize a Heisenberg-like Hamiltonian [19]. Instead of directly pursuing highly exotic magnetic states solely characterized by the absence of specific features (such as no ordering down to the lowest temperature or absence of magnon excitations), a more productive strategy has emerged. Specifically, the study of magnetically ordered or disordered compounds near a quantum critical point has proven to be fruitful. A notable example is the well-

studied compound $\text{Ba}_3\text{CoSb}_2\text{O}_9$ that realizes an effective spin-1/2 triangular antiferromagnet with XXZ model interactions, exhibiting a 120° Néel order below $T_N = 3.8\text{K}$ [20–24]. In INS experiments conducted below T_N , an unusual spectrum was observed, comprising low-lying energy collective excitations (magnonic-like) coexisting with two dispersive continua at higher energies across the entire Brillouin zone (BZ). The semiclassical theory (large- S) [23, 25, 26] falls short in explaining this spectrum, leading to speculation that $\text{Ba}_3\text{CoSb}_2\text{O}_9$ is proximate to a quantum melting point. Figure 1 schematically depicts the possible location of $\text{Ba}_3\text{CoSb}_2\text{O}_9$ with respect to a quantum critical point in a magnetic phase diagram.

Subsequent theoretical studies, including numerical tensor network calculations [27] and $1/\mathcal{N}$ Schwinger boson (SB) calculations [28], support the XXZ model. Furthermore, the SB theory provides a novel interpretation of the spectrum, suggesting that the low-lying energy magnetic excitations consist of two spinon bound states, glued by emergent (Hubbard-Stratonovich) gauge fields. These coexist with two high-energy dispersing continua made of two quasi-free spinons. Namely, at high energies, the confinement length of spinons is greater than unit space lattice. In the light of these findings, it can be concluded that in the proximity of a quantum melting point, the spin-1 collective excitation of the 120° Néel order seems better described by a bound state of two spin- $\frac{1}{2}$ spinons —the quasiparticles of the neighboring spin liquid— than the usual magnonic excitations [29, 30].

More recently [33], the delafossite material KYbSe_2 , which realizes the $J_1 - J_2$ model on the triangular lattice, has been shown to be proximate to a quantum critical point. In this study, the magnetic spectrum was observed with INS at $T = 300$ mK, slightly above the Néel temperature $T_N = 290$ mK. The spectrum displayed an extended continuum with a sharp lower edge that is gapless at the momentum K , corresponding to the 120° Néel order expected below T_N . The dynamical structure

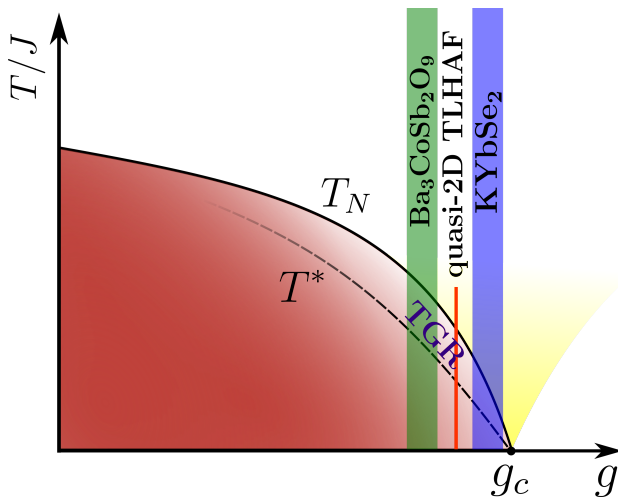


FIG. 1. Schematic phase diagram for quasi-2D frustrated antiferromagnets [31, 32]. The abscissa axis ‘ g ’ represents a generic measure of zero-point quantum fluctuations, with ‘ g_c ’ connecting continuously the 120° Néel state to a quantum spin liquid state at $T = 0$. Solid line denote the transition from the classical renormalized to the quantum critical regime, marked by the Néel temperature (T_N). The dashed line indicates the crossover around T^* from the classical renormalized regime—with well-defined two-spinon bound states across the Brillouin zone—to an intermediate regime where bound states begin to break up. This region, termed the terminated Goldstone regime (TGR) retains only bound states around the Goldstone modes. The blue and green vertical bands depict the estimated positions of named compounds in the phase diagram. The solid red line represents the location of the model used in our calculations (see Section II) and the yellow region, emerging from g_c , denote a quantum critical regime.

factor at the magnetic wave vector K exhibits a scaling collapse in $\hbar\omega/k_B T$ down to 0.3K, indicative of a second-order quantum phase transition. The agreement with theoretical predictions based on tensor network and $1/\mathcal{N}$ SB calculations suggests that KYbSe₂ is even closer to a quantum critical point than Ba₃CoSb₂O₉ (see Fig. 1). Based on the zero temperature SB prediction, it is expected that the low-energy edge of the spectrum observed at 0.3K (greater than T_N) will separate from the continuum as temperature passes through the Néel temperature down, giving rise to collective excitations made of two spinon bound states. However, it remains unclear whether this low-lying energy band will be well-defined across the entire Brillouin zone. The consistency found between theory and experiments in KYbSe₂, along with entanglement witnesses, strongly supports the strategy of investigating the magnetic spectrum of compounds in proximity to a continuous quantum phase transition. In this case, the indications are that KYbSe₂ could be proximate to a Z_2 spin liquid state.

So far, the theoretical studies mentioned above have primarily been performed at zero temperature, while only a few studies consider finite temperature [34–36]. To provide a more comprehensive description aligning with ex-

perimental conditions, the next step is to incorporate the combined effects of both interlayer exchange coupling and temperature. In compounds like Ba₃CoSb₂O₉ and KYbSe₂, although the interlayer interaction is significantly weaker than the intralayer coupling, it plays a crucial role in establishing a finite Néel temperature.

In this work, we investigate the temperature effect on the magnetic excitation spectra of spin 1/2 quasi-2D triangular AF. Unlike spin wave theory, the Schwinger boson theory (SBT) relies on magnetic link degrees of freedom that are believed to take better into account the mixing of transverse and longitudinal fluctuations, as soon as Néel temperature is approached. Firstly, we find that at the saddle point (SP) level the SBT recovers qualitatively well the expected (static) behavior of the 120° magnetically ordered regime below Néel temperature. Secondly, at the $1/\mathcal{N}$ approximation level, we have found an intriguing temperature dependence of the spectrum. Specifically, we identify a low-temperature regime, below a crossover temperature T^* , where the two-spinon bound state band is well-defined across an ample region of the Brillouin zone. However, as temperature rises above T^* , the gauge field fluctuations fail to form the two-spinon bound states in a significant region of the Brillouin zone. This leads to a differentiation in the magnetic excitation spectrum. Remarkably, for temperatures around T_N , only two spinon bound states, centered around the Goldstone modes, remain well-defined. This behavior is similar to what happens in weakly 3D interacting antiferromagnetic chains [37]. In these systems, clear signatures of quantum criticality are observed in the renormalized classical regime (below but close to the Néel temperature). In analogy to the superfluid ⁴He case, where phonon excitations terminate at some momentum and energy by decaying into two roton excitations, we call this antiferromagnetic region—between T^* and T_N —*terminated Goldstone regime* (TGR) (see Fig. 1), although the decay mechanisms are different [38]. These finite temperature results strongly support the proposed behavior of frustrated antiferromagnets near a quantum critical regime by Chubukov, Sachdev, and Senthil [31], and provide a deeper insight into the fractionalization process [39].

In Section II, we briefly developed the $1/\mathcal{N}$ Schwinger boson formalism. Section III includes the interlayer coupling, enabling the study of the Néel temperature. In Section IV, we analyze the effect of temperature on the magnetic excitation spectrum. Section V concludes with final remarks.

II. SCHWINGER BOSON FORMALISM

In this section we extend the $1/\mathcal{N}$ SB theory to finite temperatures for quasi two dimensional systems. In order to get a self contained description we present the main steps of the calculation, emphasizing the temperature dependence of the results. The details of the full calculation can be found in Ref.[30, 40–43].

We study the Heisenberg Hamiltonian in the layered triangular lattice

$$\hat{H} = \sum_{\langle ij \rangle} J_{ij} \hat{\mathbf{S}}_i \cdot \hat{\mathbf{S}}_j, \quad (1)$$

where $\langle ij \rangle$ sums over all the nearest-neighbor pairs of spins of the layered triangular lattice. The in-plane exchange interaction is J while there is a no frustrating interlayer exchange interaction J_{\perp} . For simplicity, here we study the isotropic Heisenberg model with only nearest-neighbor couplings. However, the theory can be straightforwardly extended to include anisotropic [28] and further exchange interactions [33]. In fact, in the next Section, we will present some Néel temperature estimations for real compounds with more evolved Hamiltonian than the isotropic Heisenberg model.

Within the SB formalism the Heisenberg Hamiltonian (1) can be written exactly as

$$\hat{H} = \sum_{\langle ij \rangle} J_{ij} \left(: \hat{B}_{ij}^{\dagger} \hat{B}_{ij} : - \hat{A}_{ij}^{\dagger} \hat{A}_{ij} \right), \quad (2)$$

where $\hat{A}_{ij} = \frac{1}{2}(\hat{b}_{i\uparrow}\hat{b}_{j\downarrow} - \hat{b}_{i\downarrow}\hat{b}_{j\uparrow})$ and $\hat{B}_{ij} = \frac{1}{2}(\hat{b}_{i\uparrow}\hat{b}_{j\downarrow}^{\dagger} + \hat{b}_{i\downarrow}\hat{b}_{j\uparrow}^{\dagger})$ are the SU(2) invariant link operators of the theory. A_{ij}^{\dagger} creates singlets between ij sites and B_{ij}^{\dagger} makes them resonate. Furthermore, up to a constant, $: \hat{B}_{ij}^{\dagger} \hat{B}_{ij} : \sim (\hat{\mathbf{S}}_i + \hat{\mathbf{S}}_j)^2$ and $\hat{A}_{ij}^{\dagger} \hat{A}_{ij} \sim (\hat{\mathbf{S}}_i - \hat{\mathbf{S}}_j)^2$ which gives a measure of ferromagnetic and antiferromagnetic correlations, respectively. Namely, the particular structure of Hamiltonian (2) is ideal to treat Heisenberg models in the presence of magnetic frustration [30, 44–46].

The partition function for the model is expressed as the following path integral over the coherent states of the SB's

$$\mathcal{Z}[j] = \int \mathcal{D}[\bar{b}, b] \mathcal{D}[\lambda] e^{-\int_0^{\beta} d\tau [\sum_{i\sigma} \bar{b}_{i\sigma}^{\tau} \partial_{\tau} b_{i\sigma} + \mathcal{H}(\bar{b}, b) + \mathcal{J}_b + \mathcal{J}_s]} \times e^{-\int_0^{\beta} d\tau \sum_i \lambda_i^{\tau} (\sum_{\sigma} \bar{b}_{i\sigma}^{\tau} b_{i\sigma} - 2S)}, \quad (3)$$

where $\mathcal{H}(\bar{b}, b)$ is the Hamiltonian evaluated at the site i and time τ dependent complex eigenvalues of the coherent states, $\mathcal{J}_b = \frac{1}{2} \sum_i h_i^{\mu} \mathbf{b}_i^{\tau\dagger} \cdot \sigma^{\mu} \cdot \mathbf{b}_i^{\tau}$ –with $\mathbf{b}_i^{\tau\dagger} = (\bar{b}_{i\uparrow}^{\tau}, \bar{b}_{i\downarrow}^{\tau})$ – is the coupling between the spins and an infinitesimal symmetry breaking field $\mathbf{h}_i = h(\cos(\mathbf{Q} \cdot \mathbf{r}_i), \sin(\mathbf{Q} \cdot \mathbf{r}_i), 0)$ that selects the 120° Néel order in the x-y plane $[\mathbf{Q} = (\frac{2}{3}\pi, \frac{2}{\sqrt{3}}\pi, \pi)]$, $\mathcal{J}_s = \frac{1}{2} \sum_i j_i^{\tau\mu} \mathbf{b}_i^{\tau\dagger} \cdot \sigma^{\mu} \cdot \mathbf{b}_i^{\tau}$ is the coupling between the spins and a external magnetic field $j_i^{\tau\mu}$ used to compute the dynamical spin susceptibility, and λ_i^{τ} are the Lagrange multipliers introduced to satisfy the local constraints $b_{i\uparrow}^{\dagger} b_{j\uparrow} + b_{i\downarrow}^{\dagger} b_{j\downarrow} = 2S$.

The standard procedure involves i) a Hubbard-Stratonovich (HS) transformation to decouple the $A_{ij}^{\dagger} A_{ij}$

and $B_{ij}^{\dagger} B_{ij}$ terms (quartic in bosons) of $\mathcal{H}(\bar{b}, b)$, ii) use a local reference quantization axis for the spinors $b_{i\sigma}^{\tau}$ oriented in the direction of the 120° magnetic order \mathbf{Q} , iii) integrate out the quadratic bosonic part giving rise to

$$\mathcal{Z}_{\text{bos}}(\bar{W}, W, \lambda, j) = \int \mathcal{D}[\bar{b}, b] e^{-\bar{b}^{\dagger} \cdot \mathcal{G}^{-1}(\bar{W}, W, \lambda, j) \cdot \bar{b}} = \det [\mathcal{G}(\bar{W}, W, \lambda, j)],$$

where \bar{b} is a four component vector containing the variables $b_{i\sigma}^{\tau}$ and $\bar{b}_{i\sigma}^{\tau}$, \mathcal{G}^{-1} is the 4×4 dynamical matrix (see next subsection), and $W_{ij}^{\xi\tau}$ (with $\xi = A, B$) are the HS auxiliary fields, and finally iv) exponentiate $\mathcal{Z}_{\text{bos}}(\bar{W}, W, \lambda, j)$, rendering the total partition function as

$$\mathcal{Z}[j] = \int \mathcal{D}[\bar{W}, W] \mathcal{D}[\lambda] e^{-S_{\text{eff}}(\bar{W}, W, \lambda, h, j)} \quad (4)$$

with

$$S_{\text{eff}}(\bar{W}, W, \lambda, h, j) = S_0(\bar{W}, W, \lambda) + S_{\text{bos}}(\bar{W}, W, \lambda, h, j)$$

where

$$S_0(\bar{W}, W, \lambda) = \int_0^{\beta} d\tau \left(\sum_{ij, \xi} J_{ij} \bar{W}_{ij}^{\xi\tau} W_{ij}^{\xi\tau} - i2S \sum_i \lambda_i^{\tau} \right) \quad (5)$$

and

$$S_{\text{bos}}(\bar{W}, W, \lambda, j) = -\frac{1}{2} \ln \mathcal{Z}_{\text{bos}}(\bar{W}, W, \lambda, j) = \frac{1}{2} \text{Tr} \ln [\mathcal{G}^{-1}(\bar{W}, W, \lambda, j)], \quad (6)$$

with the trace, in the last line, taken over space, time, and boson flavor indices. Equation (4) means that the interacting spin problem has been mapped exactly to a problem of free spin- $\frac{1}{2}$ bosons interacting with fluctuating (space and time) auxiliary fields $W_{ij}^{A\tau}$, $W_{ij}^{B\tau}$, and λ_i^{τ} which are the gauge fields of the theory [30].

Next, a saddle point expansion is performed and, keeping up to the Gaussian fluctuations of the auxiliary fields, the partition function yields

$$\mathcal{Z}^{(2)}[j] = e^{-S_{\text{eff}}^{\text{sp}}(\bar{W}_{\text{sp}}, W_{\text{sp}}, \lambda_{\text{sp}}, j)} \times \int \mathcal{D}[\bar{\phi}, \phi] e^{-\Delta \bar{\phi}^{\dagger} \cdot S^{(2)} \cdot \Delta \bar{\phi}}, \quad (7)$$

where the first exponential is the partition function within the SP approximation, and the integral corresponds to the contribution of the Gaussian fluctuations of the auxiliary fields $\Delta \bar{\phi}^{\dagger} = \bar{\phi}^{\dagger} - \bar{\phi}^{\text{sp}\dagger}$ with $\bar{\phi}^{\dagger} = (\bar{W}_{i,\delta}^{\xi\tau}, W_{i,\delta}^{\xi\tau}, \lambda_i^{\tau})$. $S^{(2)}$ is the fluctuation matrix composed by the second derivatives of the effective action S_{eff} with respect to the auxiliary fields [30]. It is worth to stress that once the SB theory is extended to a large \mathcal{N} number of flavors, the contribution of Gaussian fluctuations to the dynamical spin susceptibility is of order $1/\mathcal{N}$, so that, we call the present theory $1/\mathcal{N}$ SB theory although we are working within the physical case $\mathcal{N} = 2$ [40, 41, 43].

A. Saddle point equations

The SP approximation requires that

$$\frac{\partial S_{eff}}{\partial \phi_\alpha} \Big|_{sp} = \frac{\partial S_0}{\partial \phi_\alpha} \Big|_{sp} + \frac{1}{2} \text{Tr} \left[\mathcal{G}_{sp} \frac{\partial \mathcal{G}^{-1}}{\partial \phi_\alpha} \Big|_{sp} \right] = 0. \quad (8)$$

$$\mathcal{G}_{sp}^{-1}(\mathbf{k}, i\omega) = \begin{pmatrix} \left((i\omega + \lambda_{sp} + \gamma_{\mathbf{k}+\frac{\mathbf{Q}}{2}}^B) e^{-i\omega 0^+} & -\gamma_{\mathbf{k}+\frac{\mathbf{Q}}{2}}^A & \frac{1}{2} & 0 \\ -\gamma_{\mathbf{k}+\frac{\mathbf{Q}}{2}}^A & (-i\omega + \lambda_{sp} + \gamma_{\mathbf{k}+\frac{\mathbf{Q}}{2}}^B) e^{i\omega 0^+} & 0 & \frac{1}{2} \\ \frac{1}{2} & 0 & (i\omega + \lambda_{sp} + \gamma_{-\mathbf{k}+\frac{\mathbf{Q}}{2}}^B) e^{-i\omega 0^+} & -\gamma_{-\mathbf{k}+\frac{\mathbf{Q}}{2}}^A \\ 0 & \frac{1}{2} & -\gamma_{-\mathbf{k}+\frac{\mathbf{Q}}{2}}^A & (-i\omega + \lambda_{sp} + \gamma_{-\mathbf{k}+\frac{\mathbf{Q}}{2}}^B) e^{i\omega 0^+} \end{pmatrix} \quad (9)$$

with functions $\gamma_{\mathbf{k}}^A = \sum_{\delta>0} J_\delta A_\delta \sin(\mathbf{k} \cdot \delta)$ and $\gamma_{\mathbf{k}}^B = \sum_{\delta>0} J_\delta B_\delta \cos(\mathbf{k} \cdot \delta)$. Convergence factors $e^{\pm i\omega 0^+}$ are necessary to correctly take into account the temporal ordering within the functional integral. The inverse of the dynamical matrix at the SP is the spinon propagator \mathcal{G}_{sp} that can be decomposed in term of simple fractions as

$$\mathcal{G}_{sp}(\mathbf{k}, i\omega) = \sum_{\sigma\sigma'} \frac{g^{\sigma\sigma'}(\mathbf{k})}{i\omega + \sigma\varepsilon_{\mathbf{k}}^{\sigma'}(h)} \quad (10)$$

whose poles are the dispersion relations of the free spinons $\varepsilon_{\mathbf{k}}^\sigma(h)$, with $\sigma, \sigma' = \pm$, that can be obtained together with the matrices $g^{\sigma\sigma'}$ after performing a paraunitary diagonalization of the dynamical matrix (See Appendix A). Replacing the expressions of \mathcal{G}_{sp}^{-1} and \mathcal{G}_{sp} in the SP equation (8), and carrying out the Matsubara sums, we arrive at the self-consistent set of equations

$$A_\delta = \frac{1}{2N_s} \sum_{\mathbf{k}} \tilde{A}_{\mathbf{k}} \sin(\mathbf{k} + \frac{\mathbf{Q}}{2}) \cdot \delta \quad (11)$$

$$B_\delta = \frac{1}{2N_s} \sum_{\mathbf{k}} \tilde{B}_{\mathbf{k}} \cos(\mathbf{k} + \frac{\mathbf{Q}}{2}) \cdot \delta \quad (12)$$

$$S = \frac{1}{2N_s} \sum_{\mathbf{k}} \tilde{B}_{\mathbf{k}} \quad (13)$$

where N_s is the total number of sites and

$$\begin{aligned} \tilde{A}_{\mathbf{k}} &= \sum_{\sigma\sigma'} \left(g_{21}^{\sigma\sigma'}(\mathbf{k}) + g_{43}^{\sigma\sigma'}(-\mathbf{k}) \right) \left[1 + n(\sigma\varepsilon_{\mathbf{k}}^{\sigma'}(h)) \right] \\ \tilde{B}_{\mathbf{k}} &= \sum_{\sigma\sigma'} g_{11}^{\sigma\sigma'}(\mathbf{k}) n(\sigma\varepsilon_{\mathbf{k}}^{\sigma'}(h)) + g_{22}^{\sigma\sigma'}(\mathbf{k}) \left[1 + n(\sigma\varepsilon_{\mathbf{k}}^{\sigma'}(h)) \right]. \end{aligned} \quad (14)$$

The explicit temperature dependence is present in the Bose occupation numbers n .

where ϕ_α represents a given HS field (including λ) at some position and time. Taking the *ansatz* compatible with the magnetic order in the xy plane $\langle A_\delta \rangle = -\langle \bar{A}_\delta \rangle = iA_\delta$, $\langle B_\delta \rangle = \langle \bar{B}_\delta \rangle = B_\delta$ (δ represents the vector that connects sites i and j) and $\lambda_{sp} = i\lambda$, the dynamical matrix in the frequency and momentum representation, using the spinor basis $\mathbf{b}_{\mathbf{k}}^{\omega\dagger} = (\bar{b}_{\mathbf{k}\uparrow}^\omega, b_{-\mathbf{k}\downarrow}^{-\omega}, \bar{b}_{\mathbf{k}\downarrow}^\omega, b_{-\mathbf{k}\uparrow}^{-\omega})$, is written as

B. Dynamical spin susceptibility

The dynamical spin susceptibility is obtained as [30, 41]

$$\chi_{\mu\nu}(\mathbf{q}, i\omega) = \lim_{h \rightarrow 0} \lim_{N_s \rightarrow \infty} \frac{\partial^2 \ln \mathcal{Z}[j]}{\partial j_{\mathbf{q}, i\omega}^\mu \partial j_{-\mathbf{q}, -i\omega}^\nu} \Big|_{j=0}, \quad (15)$$

where the order of the limits is a key point of the calculation since we are interested in the excitation spectrum of magnetically ordered states proximate to a quantum melting point. In particular, to compute the dynamical spin susceptibility up to Gaussian order –above the SP solution– $\mathcal{Z}^{(2)}[j]$ of Eq. (7) is plugged in Eq. (15), giving rise to three terms of order $1/\mathcal{N}$. In Refs. [30, 43] we have shown that by only keeping the bubble like diagram the dynamical susceptibility can be written as

$$\chi_{\mu\mu}(\mathbf{q}, i\omega) = \chi_{\mu\mu}^{sp}(\mathbf{q}, i\omega) + \chi_{\mu\mu}^{fl}(\mathbf{q}, i\omega), \quad (16)$$

being

$$\chi_{\mu\mu}^{sp}(\mathbf{q}, i\omega) = \frac{1}{2} \text{Tr} \left[\mathcal{G}_{sp} \frac{\partial \mathcal{G}^{-1}}{\partial j_{\mathbf{q}, i\omega}^\mu} \Big|_{sp} \mathcal{G}_{sp} \frac{\partial \mathcal{G}^{-1}}{\partial j_{-\mathbf{q}, -i\omega}^\mu} \Big|_{sp} \right] \quad (17)$$

and

$$\chi_{\mu\mu}^{fl}(\mathbf{q}, i\omega) = \sum_{\alpha_1\alpha_2} \Lambda_{\phi_{\alpha_1}}^\mu(\mathbf{q}, i\omega) \mathcal{D}_{\alpha_2\alpha_1}(\mathbf{q}, i\omega) \Lambda_{\phi_{\alpha_2}}^\mu(-\mathbf{q}, -i\omega) \quad (18)$$

where

$$\Lambda_{\phi_{\alpha_i}}^\mu(\mathbf{q}, i\omega) = \frac{1}{2} \text{Tr} \left[\mathcal{G}_{sp} \frac{\partial \mathcal{G}^{-1}}{\partial \phi_{\alpha_i}} \Big|_{sp} \mathcal{G}_{sp} \frac{\partial \mathcal{G}^{-1}}{\partial j_{\mathbf{q}, i\omega}^\mu} \Big|_{sp} \right], \quad (19)$$

and $\mathcal{D}_{\alpha_1\alpha_2}$ is the inverse of the fluctuation matrix $S_{\alpha_1\alpha_2}^{(2)} = \frac{1}{2} \frac{\partial^2 S_{eff}}{\partial \phi_{\alpha_1} \partial \phi_{\alpha_2}} \Big|_{sp} = \frac{1}{2} \left\{ \frac{\partial^2 S_0}{\partial \phi_{\alpha_1} \partial \phi_{\alpha_2}} - \Pi_{\alpha_1\alpha_2} \right\}$ with

$$\Pi_{\alpha_1\alpha_2} = \frac{1}{2} \text{Tr} \left[\mathcal{G}_{sp} \frac{\partial \mathcal{G}^{-1}}{\partial \phi_{\alpha_1}} \Big|_{sp} \mathcal{G}_{sp} \frac{\partial \mathcal{G}^{-1}}{\partial \phi_{\alpha_2}} \Big|_{sp} \right]. \quad (20)$$

After carrying out the Matsubara's frequency sums in (17), (19) and (20) for the out of plane zz entry of the susceptibility, we arrive at

$$\chi_{zz}^{sp}(\mathbf{q}, i\omega) = \frac{1}{8N_s} \sum_{\mathbf{k}} \sum_{\sigma\sigma'\sigma''} \left\{ \frac{\text{Tr} \left[g^{\sigma\sigma'}(\mathbf{k}+\mathbf{q}) u^z g^{\sigma\sigma''}(\mathbf{k}) u^z \right]}{\varepsilon_{\mathbf{k}+\mathbf{q}}^{\sigma'} - \varepsilon_{\mathbf{k}}^{\sigma''} + \sigma i\omega} \left(n(\varepsilon_{\mathbf{k}}^{\sigma''}) - n(\varepsilon_{\mathbf{k}+\mathbf{q}}^{\sigma'}) \right) - \frac{\text{Tr} \left[g^{\sigma\sigma'}(\mathbf{k}+\mathbf{q}) u^z g^{\bar{\sigma}\bar{\sigma}''}(\mathbf{k}) u^z \right]}{\varepsilon_{\mathbf{k}+\mathbf{q}}^{\sigma'} + \varepsilon_{\mathbf{k}}^{\sigma''} + \sigma i\omega} \left(n(\varepsilon_{\mathbf{k}}^{\sigma''}) + n(\varepsilon_{\mathbf{k}+\mathbf{q}}^{\sigma'}) + 1 \right) \right\} \quad (21)$$

$$\Lambda_{\phi_{\alpha_1}}^z(\mathbf{q}, i\omega) = \frac{1}{4N_s} \sum_{\mathbf{k}} \sum_{\sigma\sigma'\sigma''} \left\{ \frac{\text{Tr} \left[g^{\sigma\sigma'}(\mathbf{k}+\mathbf{q}) u^z g^{\sigma\sigma''}(\mathbf{k}) v_{\phi_{\alpha_1}}^{\mathbf{k}, \mathbf{k}+\mathbf{q}} \right]}{\varepsilon_{\mathbf{k}+\mathbf{q}}^{\sigma'} - \varepsilon_{\mathbf{k}}^{\sigma''} + \sigma i\omega} \left(n(\varepsilon_{\mathbf{k}}^{\sigma''}) - n(\varepsilon_{\mathbf{k}+\mathbf{q}}^{\sigma'}) \right) - \frac{\text{Tr} \left[g^{\sigma\sigma'}(\mathbf{k}+\mathbf{q}) u^z g^{\bar{\sigma}\bar{\sigma}''}(\mathbf{k}) v_{\phi_{\alpha_1}}^{\mathbf{k}, \mathbf{k}+\mathbf{q}} \right]}{\varepsilon_{\mathbf{k}+\mathbf{q}}^{\sigma'} + \varepsilon_{\mathbf{k}}^{\sigma''} + \sigma i\omega} \left(n(\varepsilon_{\mathbf{k}}^{\sigma''}) + n(\varepsilon_{\mathbf{k}+\mathbf{q}}^{\sigma'}) + 1 \right) \right\} \quad (22)$$

$$\Pi_{\alpha_1\alpha_2}(\mathbf{q}, i\omega) = \frac{1}{2N_s} \sum_{\mathbf{k}} \sum_{\sigma\sigma'\sigma''} \left\{ \frac{\text{Tr} \left[g^{\sigma\sigma'}(\mathbf{k}+\mathbf{q}) v_{\phi_{\alpha_1}}^{\mathbf{k}+\mathbf{q}, \mathbf{k}} g^{\sigma\sigma''}(\mathbf{k}) v_{\phi_{\alpha_2}}^{\mathbf{k}, \mathbf{k}+\mathbf{q}} \right]}{\varepsilon_{\mathbf{k}+\mathbf{q}}^{\sigma'} - \varepsilon_{\mathbf{k}}^{\sigma''} + \sigma i\omega} \left(n(\varepsilon_{\mathbf{k}}^{\sigma''}) - n(\varepsilon_{\mathbf{k}+\mathbf{q}}^{\sigma'}) \right) - \frac{\text{Tr} \left[g^{\sigma\sigma'}(\mathbf{k}+\mathbf{q}) v_{\phi_{\alpha_1}}^{\mathbf{k}+\mathbf{q}, \mathbf{k}} g^{\bar{\sigma}\bar{\sigma}''}(\mathbf{k}) v_{\phi_{\alpha_2}}^{\mathbf{k}, \mathbf{k}+\mathbf{q}} \right]}{\varepsilon_{\mathbf{k}+\mathbf{q}}^{\sigma'} + \varepsilon_{\mathbf{k}}^{\sigma''} + \sigma i\omega} \left(n(\varepsilon_{\mathbf{k}}^{\sigma''}) + n(\varepsilon_{\mathbf{k}+\mathbf{q}}^{\sigma'}) + 1 \right) \right\} \quad (23)$$

where $u_z = \text{diag}(1, -1, -1, 1)$ come from the external vertices $\frac{\partial \mathcal{G}^{-1}}{\partial j_{\mathbf{q}, i\omega}^u}$ and $v_{\phi_{\alpha}}^{\mathbf{k}, \mathbf{k}'}$ come from the internal vertices $\frac{\partial \mathcal{G}^{-1}}{\partial \phi_{\alpha}}$. Similar expressions can be obtained for the in-plane (xx and yy) entries of the susceptibility.

Finally, by means of the fluctuation-dissipation theorem, we can obtain the dynamical spin structure factor by performing the analytic continuation $i\omega \rightarrow \omega + i\eta$ in the dynamical spin susceptibility

$$S^{\mu\mu}(\mathbf{q}, \omega) = \left(\frac{-1}{\pi} \right) \frac{1}{1 - e^{-\beta\omega}} \text{Im}[\chi^{\mu\mu}(\mathbf{q}, \omega + i\eta)], \quad (24)$$

where η is the artificial broadening.

III. MAGNETICALLY ORDERED REGIME

In this section we focus on the ability of the SBT to describe the finite temperature behavior as a function of J_{\perp} . In particular, in the ordered regime, we find that the SP solution recovers qualitatively well the expected (static) behavior of quasi-2D triangular AFs.

In accordance with the Mermin-Wagner theorem [40, 41], the onset of long-range magnetic order in a triangular Heisenberg antiferromagnet –with continuous symmetry and short range exchange interactions– can only

occur at zero temperature. Correspondingly, by mapping the 2D Heisenberg antiferromagnet to the effective non linear sigma model (NLSM), it is shown that there is a crossover from a high temperature paramagnetic regime to a low temperature classical renormalized regime where the finite temperature spin correlation functions increases exponentially as temperature goes down to zero [47]. The SBT reproduces quite well this low temperature behavior of the spin correlations at the saddle point level [31, 48]. In particular, it recovers the low temperature 120° Néel correlation functions predicted by NLSM, while at zero temperature the condensation of the SBs signals the occurrence of a finite magnetization. At higher temperatures, however, the SP approximation overestimates the entropy –due to violation of the local constraint– so neighboring spins become perfectly uncorrelated at certain temperature [49]. This unphysical result has been studied in the context of large \mathcal{N} theory along with the possibility of being corrected for finite \mathcal{N} [50].

On the other hand, any finite interlayer exchange J_{\perp} gives rise to long range magnetic order below a finite Néel temperature. The very definition of a quasi-2D antiferromagnet implies that J_{\perp} is much smaller than the in-plane exchange interaction J –two or more orders of magnitude smaller–, making it difficult to model the compounds in order to extract J_{\perp} values from the measured Néel temperatures.

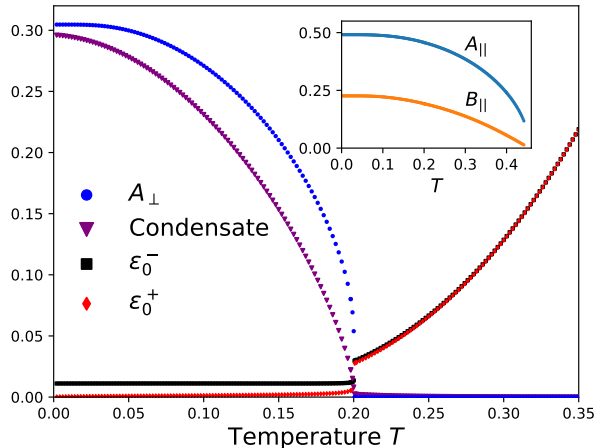


FIG. 2. A_{\perp} (blue circles), condensate (purple triangles), $\sigma = +$ (red diamonds) and $\sigma = -$ (black squares) spinon dispersion relation gaps as a function of the temperature for $N_s = 144 \times 144 \times 8$ sites and $J_{\perp} = 0.01J$. Inset: Temperature dependence of the in-plane saddle point parameters A_{\parallel} and B_{\parallel} .

Formally, the magnetic phase transition is derived by studying the behavior of the SB self consistent Eqs. (11-13) in the thermodynamic limit, namely, first taking $N_s \rightarrow \infty$ and then $h \rightarrow 0$ [41]. In particular, there is a regime where $\varepsilon_{\mathbf{0}}^+ \rightarrow 0$ and $\varepsilon_{\mathbf{0}}^- \neq 0$ which corresponds to the condensation of the SB $\sigma = +$ at $\mathbf{q} = 0$. This condensation is directly related to the presence of a local magnetization that lies in the xy plane and points in the x direction of a local reference frame that rotates 120° from site to site. In practice, this calculations is carried out on finite size systems of $N_s = N_{\perp} \times N_{\parallel}$ sites, where N_{\perp} is the number of layers taken and N_{\parallel} is the number of sites in each triangular lattice layer. Then, a symmetry breaking field $h = 1/N_{\parallel}$ is applied. Since $\varepsilon_{\mathbf{0}}^+ \sim 1/N_{\parallel}$ and $\varepsilon_{\mathbf{0}}^- \sim (1/N_{\parallel})^{\frac{1}{2}}$, the condensate is identified with the $\mathbf{q} = 0$ and $+$ term of the constraint equation (13). Fig. 2 shows the dependence of this condensate with temperature for a quasi-2D triangular system composed by 8 layers –with periodic boundary conditions– and $J_{\perp}/J = 0.01$. In this work, we have taken $N_{\parallel} = 144 \times 144$. This figure also shows the spinon relation dispersion values $\varepsilon_{\mathbf{0}}^+$ and $\varepsilon_{\mathbf{0}}^-$ where it can be seen that $\varepsilon_{\mathbf{0}}^+ \sim 0$ (gapless) and $\varepsilon_{\mathbf{0}}^- \neq 0$ (gapped) for $T \leq T_N$ (consistent with $\sigma = +$, $\mathbf{q} = \mathbf{0}$ condensate); while for $T > T_N$, it is opened a gap in both flavors $\varepsilon_{\mathbf{0}}^+ = \varepsilon_{\mathbf{0}}^- \neq 0$ what signals no condensation, that is, the absence of magnetic order. In the next section we will see that this behavior of the condensate has a crucial effect on the magnetic spectrum as one approaches to the Néel temperature.

One way to measure the spin correlation between nearest-neighbor spins along the interlayer direction is by computing the saddle-point value of the Hubbard-

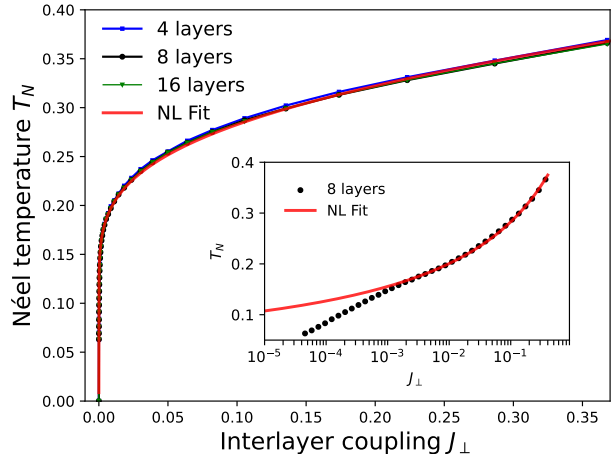


FIG. 3. Néel temperature as a function of the interlayer coupling J_{\perp} for $N_{\parallel} = 144$ and different number of layers N_{\perp} (with periodic boundary conditions). Inset: The solid red line corresponds to the non-linear fit (26) for the 8 layers SB result.

Stratonovich field A_{\perp} , through the relation

$$\langle \mathbf{S}_i \cdot \mathbf{S}_{i+c} \rangle = B_{\perp}^2 - A_{\perp}^2. \quad (25)$$

As the interlayer exchange interactions are not frustrated, B_{\perp} vanishes, signalling the antiparallel spin alignment along the perpendicular direction. The behavior of A_{\perp} versus temperature is shown in Fig. 2. There we observe that A_{\perp} behaves similar to the condensate, particularly vanishing at the Néel temperature, so that the fact that $A_{\perp} \neq 0$ is an evidence of the 3D character of the magnetic order. Namely, if $A_{\perp} \neq 0$, the system exhibits long-range magnetic order, whereas above T_N the triangular layers are magnetically decoupled ($A_{\perp} = 0$) and the local magnetization goes to zero, in accordance with Mermin-Wagner physics. In other words, the transition between the magnetically ordered and paramagnetic phase occurs due to the effective bidimensionalization of the magnetic state as temperature increases. So, the vanishing of A_{\perp} is another good signal of the Néel temperature. Notice that as the temperature increases, the spin correlations in all directions are weakened. One would expect, naively, that A_{\perp} is of the order of J_{\perp} , however any finite value of the interlayer coupling is enough to generate strong correlations between triangular layers ($A_{\perp} \simeq 0.3$ at $T = 0$).

The inset of Fig. 2 shows the dependence of the in-plane parameters A_{\parallel} and B_{\parallel} with temperature. Even if the SP solution predicts the above mentioned unphysical transition to a perfectly uncorrelated paramagnet around $T \sim 0.43J$, when $T \lesssim 0.2J$ the SP solution predicts reasonable results for the magnetically ordered regime of quasi-2D triangular AFs.

Fig. 3 shows the Néel temperature as a function of J_{\perp} and the number of triangular layers with periodic bound-

ary conditions. For very low J_{\perp} it is observed that T_N remains practically independent of the number of layers for $N_{\perp} \geq 4$, simplifying notoriously the calculation of T_N for quasi-2D systems. It is worth to stress that linear spin wave theory applied to the quasi-2D triangular AF predicts larger values of the Néel temperatures than the SBT ones [51]. For instance, for $J_{\perp}/J = 0.25$, $T_N^{LSWT}/J \sim 0.8$ while $T_N^{SBT}/J \sim 0.32$. This clearly indicates that LSWT strongly overestimates the finite temperature magnetization with respect to SBT. These values are consistent with the expected behavior near T_N , where the transverse and longitudinal fluctuations become of the same order. This feature is surely better captured by the link fields A_{ij} and B_{ij} of the SBT than the local description of LSWT. In addition, the SB results are compared with a non linear fit corresponding to the empirical formula

$$T_N(J_{\perp}) = \frac{4\pi\rho_s}{b - \ln(J_{\perp})} \quad (26)$$

based on the random phase approximation combined with quantum Monte Carlo simulations performed in unfrustrated Heisenberg AFs [52]. Here, the best fit is given by $\rho_s = 0.12675$, $b = 3.33257$. Notably, the SB results follows quite well the empirical formula down to $J_{\perp} \sim 10^{-3}$ (see inset of Fig. 3). Taking into account the complication of performing QMC calculations at very low temperatures on triangular lattices –due to sign problem– the fact that the best fit gives a value for the spin stiffness that is close to the SP result already computed at zero temperature, $\rho_s = 0.11$ [53], lends support to our procedure to estimate J_{\perp} values from T_N .

The above results for the Heisenberg model can be easily extended to the XXZ and $J_1 - J_2$ models. In both cases we have observed that T_N behaves in the expected manner, that is, for a fixed value of J_{\perp} , T_N increases as anisotropy Δ increases; whereas T_N decreases as frustration J_2/J_1 increases. In $\text{Ba}_3\text{CoSb}_2\text{O}_9$, described by the XXZ model with estimated values $J^z/J = 0.937$ and $J_{\perp}/J = 0.061$, the Néel temperature gives $T_N^{XXZ}/J = 0.274$, which should be compared with the experimental value $T_N^{\text{exp}}/J^{\text{exp}} \sim 0.2$ [25, 26, 28]. In KYbSe_2 , described by the $J_1 - J_2$ model with estimated value $J_2/J_1 = 0.05$ and the Néel temperature $T_N^{\text{exp}}/J_1^{\text{exp}} \sim 0.045$ [33] we obtain a magnitude for J_{\perp} that is smaller than 0.01% of J . This result is in line with the experimental certainty that KYbSe_2 is one of the best examples of a two dimensional triangular AF.

Finally, it is important to remark that although we do not expect to obtain a precise prediction for the values of J_{\perp} or T_N from a saddle point (mean field) approximation, the fact that the SP solution gives the expected qualitative description of finite temperature properties is crucial to compute reliable spectra (to order $1/\mathcal{N}$) in order to get a consistent thermal picture of the magnetic excitations.

IV. SPECTRA

A. Temperature evolution

In this subsection we focus on the temperature evolution of the magnetic spectra. Before, we recall our previous results regarding the zero temperature predictions of SBT for the excitation spectrum of the 2D triangular Heisenberg model [30, 43, 46]. At the saddle point level [46] the excitation spectrum consist of a two free spinon continuum (see top panel of first column of Fig 4). The lower edge of the continuum corresponds to $\min(\varepsilon_{\mathbf{k}+\mathbf{q}}^{\sigma'} + \varepsilon_{\mathbf{k}}^{\sigma})$ (see denominator in Eq. 21) and it is obtained when one spinon excitation is created in the normal phase and another in the condensate. Furthermore, due to the local constraint violation, the magnetic spectrum exhibit spurious modes (see the gapped band at momentum K) arising from unphysical density fluctuations [54]. The Gaussian correction changes drastically the SP spectrum [28, 30]: i) it cancels out both, the lower edge of the SP two spinon continuum and the spurious band and ii) it introduces new collective modes (the poles of the RPA propagator \mathcal{D}) consisting of low energy two-spinon bound states along with a quasi-free two spinon continuum at higher energy (see top panel of second column of Fig 5). These two-spinon bound states are the single-magnon excitations since, in the large S limit, we have numerically found that the $1/\mathcal{N}$ SBT spectrum coincides with the LSWT prediction [43]. Namely, in the large S limit, the two-spinon continuum vanishes and the two-spinon bound state band coincides exactly with both, the magnon band and the spectral weight predicted by LSWT. Then, for the physical case of spin 1/2, it is fair to identify the two-spinon bound state with the single-magnon excitations.

Fig. 4 displays the temperature evolution of the magnetic spectra along the Brillouin zone path shown in the $T = 0$ panel. On the left column, the saddle-point predictions are shown, and it can be seen that, there is almost no change in the structure and intensity of the spectra, except very close to the Néel temperature (bottom left panel). In contrast, the $1/\mathcal{N}$ -corrected results, shown in the right column, exhibits a non-trivial behavior with temperature. As temperature increases, a continuum signal starts filling the gap between the single-magnon dispersion and the $T = 0$ continuum, due to the thermal creation and absorption of spinons (see denominators $\varepsilon_{\mathbf{k}+\mathbf{q}}^{\sigma'} - \varepsilon_{\mathbf{k}}^{\sigma}$ in Eq. 23). These thermal processes take place at the same energy of the magnon band, destroying the coherence of the two-spinon bound states, which decay to two quasi-free spinon states. Consequently, the single-magnon excitations acquire a finite lifetime, signalled by the broadening of the magnon quasiparticle (see below). In a semiclassical picture, at $T = 0$, due to the non-collinear magnetic order, the transverse and longitudinal magnetic fluctuations are tightly coupled. Then, the effect of finite temperature is to incoherently decouple both

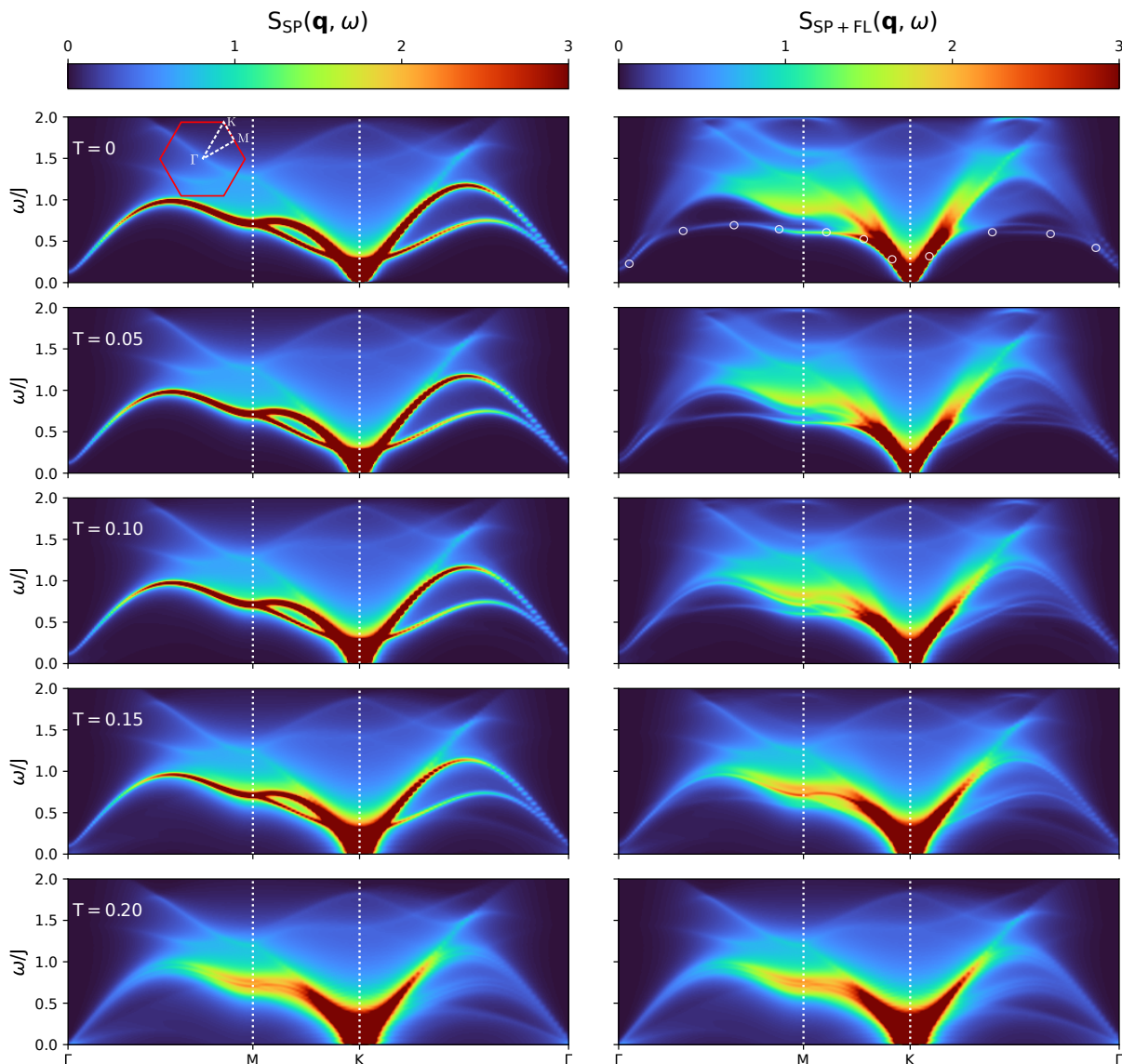


FIG. 4. Total dynamical structure factor (DSF) for the quasi-2D triangular antiferromagnet ($J_{\perp} = 0.01J$) obtained with the Schwinger boson theory at different temperatures. Left column: saddle point contribution to the DSF. Right column: saddle point plus Gaussian fluctuations contribution to the DSF. At the Néel temperature $T = 0.2J$, Gaussian fluctuations vanish and the remaining signal comes from the saddle point. Notice that there is a small gap at Γ as the spectra are computed for $k_z = \pi$. The open circles at the top right panel aid to identify the two-spinon bound state band, corresponding to the S^{zz} component. The artificial broadening is taken $\eta = 0.02$.

kind fluctuations and the $1/\mathcal{N}$ corrections correctly capture this behavior.

We identify a crossover temperature $T^* \approx 0.75T_N$, above which the magnon excitations lose their coherence across a significant region of the first Brillouin zone, due to the mentioned decay in the emergent continuum. Only in the vicinity of the Goldstone modes, magnons survive as well-defined quasiparticles. Ultimately, above the Néel temperature, the spectra becomes fully diffusive, and the $1/\mathcal{N}$ corrections to the magnetic dynamical susceptibility vanish. Notice that saddle-point and $1/\mathcal{N}$ -corrected results are practically the same (see $T = 0.20$

panel in Fig. 4). This is equivalent to saying that, when temperature is high enough, the $SU(2)$ symmetry is restored.

Figure 5 shows the component $S^{zz}(\mathbf{q}, \omega)$ of the dynamical spin structure factor along the same path of the Brillouin zone as Fig. 4. As the long-range magnetic order lies in the $x - y$ plane, $S^{zz}(\mathbf{q}, \omega)$ takes only into account transverse magnetic fluctuations, whereas the total spectra contains also the longitudinal fluctuations, that for non-collinear orders is tightly coupled with the in-plane transverse ones. It can be noticed that the relative spectral weight of the continuum signal with re-

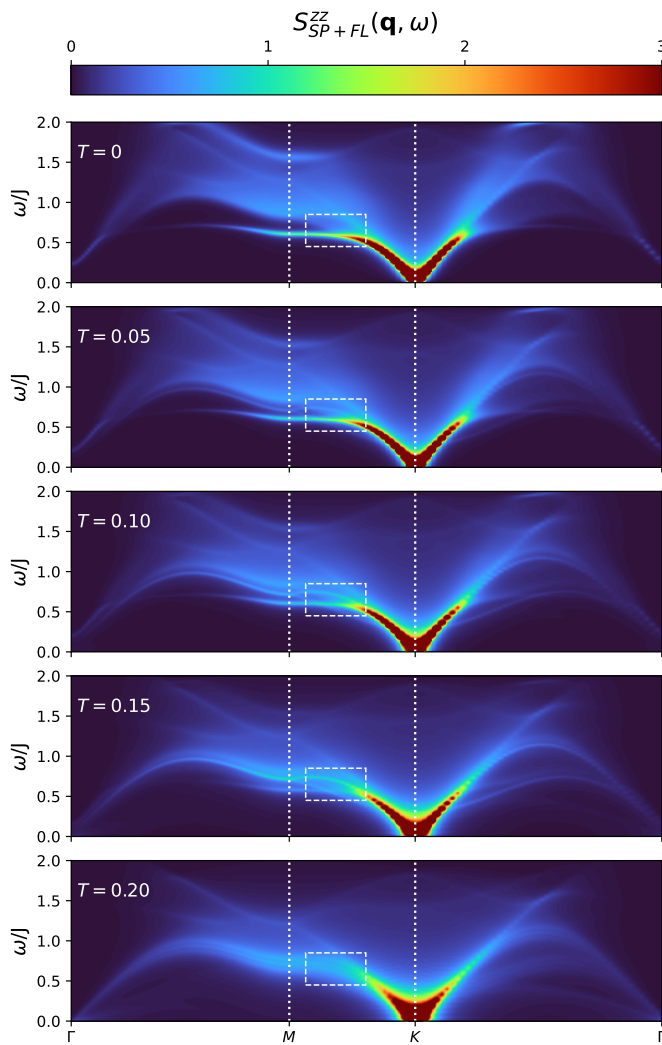


FIG. 5. Thermal evolution of the transverse dynamical structure factor $S^{zz}(\mathbf{q}, \omega)$ for the quasi 2D triangular antiferromagnet ($J_{\perp} = 0.01J$) obtained with the Schwinger boson theory. Inside the dashed square it is shown how the emergent thermal continuum mixes with the magnon band at $T = 0.15J$, producing its decay.

spect to the single-magnon signal is smaller for the zz component than for the total one (see right column in Fig. 4). In other words, the anomalous extended continua, characteristic of the triangular quantum antiferromagnet, has its origin mainly in the in-plane spin fluctuations. The white dashed square is a visual aid to help following the thermal evolution of a sector of the single-magnon dispersion, between K and M points. For low temperatures, the magnon excitations in this sector are well defined as there is almost no change with respect to $T = 0$. However, around $T^* \simeq 0.15$, the emergent thermal spinons produce the decay of the two-spinon bound states (magnons). Beyond T^* , the whole spectra become diffusive except in the neighborhood of the Goldstone modes.

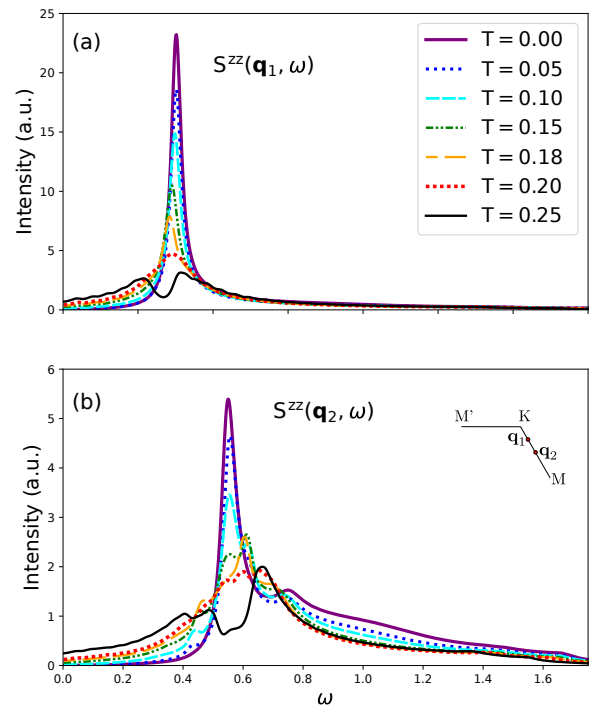


FIG. 6. Thermal evolution of the transverse dynamical structure factor $S^{zz}(\mathbf{q}, \omega)$ for (a) $\mathbf{q}_1 = (\frac{3\pi}{4}, \frac{7\pi}{4\sqrt{3}}, \pi)$ and (b) $\mathbf{q}_2 = (\frac{5\pi}{6}, \frac{3\pi}{2\sqrt{3}}, \pi)$. The two momenta are shown in a plot of the BZ path at the top right corner of the (b) panel. The magnon peak signal holds to higher temperatures for the closest momentum to the Goldstone mode, \mathbf{q}_1 . At the Néel temperature $T = 0.2J$, the fluctuations vanish completely, and the excitations are only due to free spinons.

B. Relative spectral weight of the two-spinon bound states

To support our picture about the thermal evolution of the magnons and to identify the crossover temperature, we analyze the spectral weight contribution of the two-spinon bound states and fix a criterion to quantify T^* . Fig. 6 displays $S^{zz}(\mathbf{q}, \omega)$ for two different momenta \mathbf{q}_1 and \mathbf{q}_2 . It can be seen that for \mathbf{q}_1 , close to Goldstone point K , although the magnon loses spectral weight as the temperature increases, it is always well defined, up to the Néel temperature ($T_N = 0.2$). On the other hand, for \mathbf{q}_2 between the K and M points, the quasiparticle coherence is lost for $T \gtrsim 0.15$, being its spectral weight transferred to the continuum background. This behaviour is observed in an ample region of Brillouin zone. In order to see this, in Fig. 7 we compare the magnon spectral weight with the total signal of the dynamical structure factor along the $K \rightarrow M$ path, for several temperatures. The points are computed by taking the quotient between

the spectral weight of the magnon resonance, obtained from the $1/\mathcal{N}$ -corrected $S^{zz}(\mathbf{q}, \omega)$, and the total (saddle-point plus $1/\mathcal{N}$ -corrections) spectral weight. We identify the crossover temperature T^* as the one above which, for all momenta except in the vicinity of the Goldstone modes, the magnon spectral weight goes down to 10% of the total spectral weight. A similar behavior is observed in the excitation spectrum of the superfluid ^4He , where phonon excitations terminate at some momentum by decaying into two roton excitations [38, 55]. Though the decay mechanism differs, we term this antiferromagnetic region, between T^* and T_N , the *terminated Goldstone regime* (see Fig. 1). This observation contrasts with the expectation that the magnon would persist throughout the entire Brillouin zone for non-frustrated antiferromagnets. Finally, at the Néel temperature, the whole spectra become incoherent, even at the Goldstone modes.

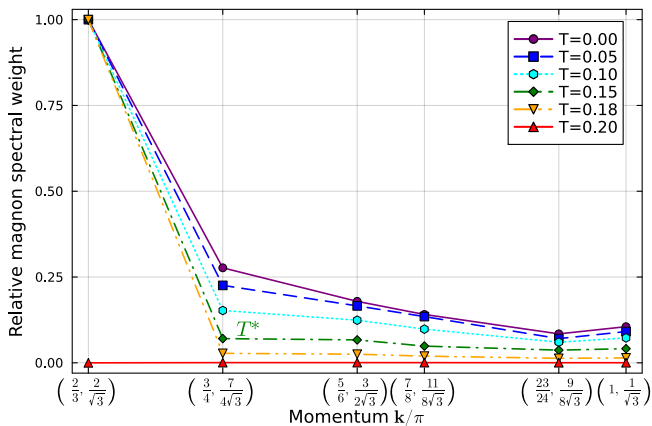


FIG. 7. Relative magnon spectral weight as a function of the temperature for some momenta \mathbf{k} on the Brillouin zone path $K = (\frac{2\pi}{3}, \frac{2\pi}{3}, \pi) \rightarrow M = (\pi, \pi/\sqrt{3}, \pi)$. On the x-axis, the component common to all points, $k_z = \pi$, is omitted.

C. Lifetime of the magnon excitations

In order to further quantify the effect of the thermal activated spinons on the two-spinon bound states, Fig. 8 shows the temperature evolution of its width for a momentum \mathbf{k} close to the Goldstone mode. While at $T = 0$ the finite width is given by twice the artificial broadening $\eta = 0.02$, necessary to perform the analytical continuation (see Eq. 24), as the temperature rises the width has a T^2 behavior (see inset). At low temperature ($T < T^*$) the lifetime hardly changes with respect to its ground state value whereas for $T > T^*$ there is a pronounced increase. This is consistent with the terminated Goldstone regime picture. It is worth to stress that the thermal evolution of the magnon lifetime has been little explored in the literature [56]. We recall that the present result is limited to two-spinon scattering processes, and if we would like to include magnon-magnon interactions, four

spinon processes should be considered [30].

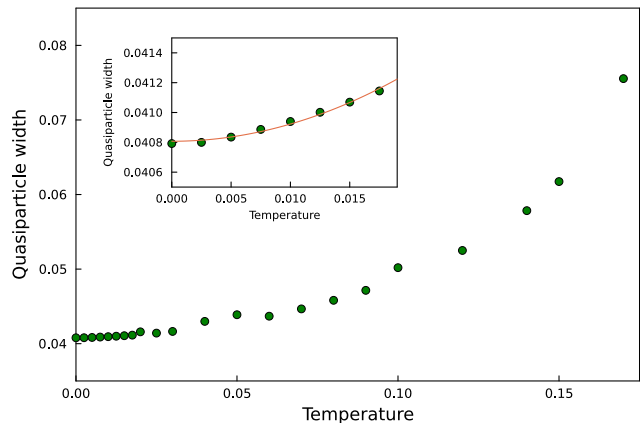


FIG. 8. Temperature dependence of the quasiparticle peak width for momentum $\mathbf{k} = (2.225, 3.4, \pi)$ which is close the Goldstone mode. Inset: Low temperature fit of the form $f(T) = aT^2 + b$, where $a = 1.1555$ and $b = 0.0408$. b is twice the artificial broadening η .

V. CONCLUDING REMARKS

Our results on the quasi-2D triangular antiferromagnet can be related with recent numerical predictions for the specific heat and entropy of the 2D triangular Heisenberg antiferromagnet [34–36]. In these studies two characteristics temperatures are found: a high temperature scale $T_h \sim 0.5J$ signalling the development of nearest-neighbor spin correlation and a low temperature scale $T_l \sim 0.2J$ related to the thermal activation of the roton excitations. We conjecture that the crossover temperature $T^* \simeq 0.75T_N$ can be associated with T_l : around $T \sim T^*$ the antiferromagnet enters the terminated Goldstone regime, where the high density of thermally activated spinons around M gives rise to the decay of the magnons away from the Goldstone points. On the other hand, the high temperature scale T_h can be associated with the “pathological” temperature $T \simeq 0.43J$ of the Schwinger boson theory [49, 50], above which the mean-field solution corresponds to an infinite temperature perfect paramagnet, in which the spin correlations vanish exactly.

In summary, in order to make contact with the experimental conditions we have studied the thermal evolution of the magnetic excitations of a quasi-2D triangular antiferromagnet, by means of a parton theory solved as a $1/\mathcal{N}$ expansion of Schwinger boson theory. Recently, this approach has been successfully applied –at zero temperature– to frustrated antiferromagnets close to a quantum critical point [28, 33]. We have found that the magnon excitations, described in our theory as two-spinon bound states, decay due to the proliferation of thermally activated spinons. The decay is very pro-

nounced in the temperature range $T^* < T < T_N$, which we have named *terminated Goldstone regime*, because – above T^* – the two-spinon bound states survive only in the vicinity of the Goldstone modes. In the quantum critical regime, above the Néel temperature, the excitations would correspond to quasi-free spinon states.

The coexistence of quantum critical features and magnon excitations, below Néel temperature, has been observed in weakly 3D interacting chains [37] and also in the triangular antiferromagnet CuCrO_2 [57]. These results give support to the idea that the fractionalization of magnons –proposed for 2D frustrated AF– near a quantum critical point [4, 8, 31, 39] can be safely extended to more realistic quasi-2D triangular antiferromagnets.

VI. ACKNOWLEDGMENTS

We thank Cristian Batista for insightful discussions. We acknowledge financial support by CONICET (Argentina) under Grant PIP No. 3220.

Appendix A: Numerical inverse of the dynamical matrix

The dynamical matrix (9) can be written as

$$\mathcal{G}_{sp}^{-1}(\mathbf{k}, i\omega) = i\omega\mathcal{S} + \mathcal{M}_{\mathbf{k}} \quad (\text{A1})$$

where we have separated the \mathbf{k} dependent terms from the ω dependent ones, and $\mathcal{S} = \text{diag}(+1, -1, +1, -1)$ is the paraunitary matrix. Then we perform a paraunitary

diagonalization of the momentum dependent part, $\mathcal{M}_{\mathbf{k}} = \mathcal{U}_{\mathbf{k}}^\dagger \mathcal{D}_{\mathbf{k}} \mathcal{U}_{\mathbf{k}}$, where $\mathcal{D}_{\mathbf{k}}$ is the diagonal matrix that contains the eigenvalues and $\mathcal{U}_{\mathbf{k}}$ is the paraunitary transformation matrix [58]. Given that \mathcal{S} is invariant under paraunitary transformations ($S = \mathcal{U}_{\mathbf{k}}^\dagger \mathcal{S} \mathcal{U}_{\mathbf{k}}$) we can write

$$\mathcal{G}_{sp}^{-1}(\mathbf{k}, i\omega) = \mathcal{U}_{\mathbf{k}}^\dagger (i\omega\mathcal{S} + \mathcal{D}_{\mathbf{k}}) \mathcal{U}_{\mathbf{k}} \quad (\text{A2})$$

and the dynamical matrix inverse is obtained as

$$\mathcal{G}_{sp}(\mathbf{k}, i\omega) = \mathcal{U}_{\mathbf{k}}^{-1} \mathcal{S} (i\omega + \mathcal{S} \mathcal{D}_{\mathbf{k}})^{-1} (\mathcal{U}_{\mathbf{k}}^\dagger)^{-1} \quad (\text{A3})$$

where

$$(i\omega + \mathcal{S} \mathcal{D}_{\mathbf{k}})^{-1} = \begin{pmatrix} \frac{1}{i\omega + \varepsilon_{\mathbf{k}}^+} & 0 & 0 & 0 \\ 0 & \frac{1}{i\omega - \varepsilon_{\mathbf{k}}^-} & 0 & 0 \\ 0 & 0 & \frac{1}{i\omega + \varepsilon_{\mathbf{k}}^-} & 0 \\ 0 & 0 & 0 & \frac{1}{i\omega - \varepsilon_{\mathbf{k}}^+} \end{pmatrix}. \quad (\text{A4})$$

The eigenvalues $\varepsilon_{\mathbf{k}}^\sigma$ structure is consistent with the $\mathbf{k} \rightarrow -\mathbf{k}$ invariance. Finally, the simple fraction decomposition of the SP Green function matrix is

$$\mathcal{G}_{sp}(\mathbf{k}, i\omega) = \sum_{\sigma\sigma'} \frac{g^{\sigma\sigma'}(\mathbf{k})}{i\omega + \sigma\varepsilon_{\mathbf{k}}^{\sigma'}} \quad (\text{A5})$$

where $\sigma, \sigma' = \pm$ and

$$\begin{aligned} g_{\alpha\beta}^{++} &= \mathcal{U}_{\alpha 1}^{-1} (\mathcal{U}^\dagger)_{1\beta}^{-1}, & g_{\alpha\beta}^{--} &= -\mathcal{U}_{\alpha 2}^{-1} (\mathcal{U}^\dagger)_{2\beta}^{-1}, \\ g_{\alpha\beta}^{+-} &= \mathcal{U}_{\alpha 3}^{-1} (\mathcal{U}^\dagger)_{3\beta}^{-1}, & g_{\alpha\beta}^{-+} &= -\mathcal{U}_{\alpha 4}^{-1} (\mathcal{U}^\dagger)_{4\beta}^{-1}. \end{aligned}$$

In the last expressions we have omitted the \mathbf{k} dependence to simplify the notation.

-
- [1] R. B. Laughlin and D. Pines, The Theory of Everything, Proceedings of the National Academy of Sciences **97**, 28 (2000).
- [2] X.-G. Wen, Choreographed entanglement dances: Topological states of quantum matter, Science **363**, 3099 (2019).
- [3] P. Anderson, Resonating valence bonds: A new kind of insulator?, Mater. Res. Bull. **8**, 153 (1973).
- [4] S. Sachdev, Quantum magnetism and criticality, Nature Physics **4**, 173 (2008).
- [5] B. Normand, Frontiers in frustrated magnetism, Contemporary Physics **50**, 533 (2009).
- [6] B. J. Powell and R. H. McKenzie, Quantum frustration in organic Mott insulators: from spin liquids to unconventional superconductors, Reports on Progress in Physics **74**, 056501 (2011).
- [7] L. Savary and L. Balents, Quantum spin liquids: a review, Rep. Prog. Phys. **80**, 016502 (2017).
- [8] Y. Zhou, K. Kanoda, and T.-K. Ng, Quantum spin liquid states, Rev. Mod. Phys. **89**, 025003 (2017).
- [9] C. Broholm, R. J. Cava, S. A. Kivelson, D. G. Nocera, M. R. Norman, and T. Senthil, Quantum spin liquids, Science **367**, 0668 (2020).
- [10] P. A. Lee, N. Nagaosa, and X.-G. Wen, Doping a Mott insulator: Physics of high-temperature superconductivity, Rev. Mod. Phys. **78**, 17 (2006).
- [11] V. Kalmeyer and R. B. Laughlin, Equivalence of the resonating-valence-bond and fractional quantum Hall states, Phys. Rev. Lett. **59**, 2095 (1987).
- [12] C. Lacroix, P. Mendels, and F. Mila, eds., *Introduction to Frustrated Magnetism: Materials, Experiments, Theory* (Springer-Verlag, Berlin Heidelberg, 2011).
- [13] T. Kim, K. Park, J. C. Leiner, and J.-G. Park, Hybridization and Decay of Magnetic Excitations in Two-Dimensional Triangular Lattice Antiferromagnets, Journal of the Physical Society of Japan **88**, 081003 (2019).
- [14] A. Tennant, Studies of Spinons, Majoranas, and Monopoles in Spin Liquid and Quantum Critical Magnets with Neutrons, Journal of the Physical Society of Japan **88**, 081009 (2019).

- [15] Y. Tokura, M. Kawasaki, and N. Nagaosa, Emergent functions of quantum materials, *Nature Physics* **13**, 1056 (2017).
- [16] B. Keimer and J. E. Moore, The physics of quantum materials, *Nature Physics* **13**, 1045 (2017).
- [17] Y. Li, YbMgGaO₄: A Triangular-Lattice Quantum Spin Liquid Candidate, *Advanced Quantum Technologies* **2**, 1900089 (2019).
- [18] J. Wen, S.-L. Yu, S. Li, W. Yu, and J.-X. Li, Experimental identification of quantum spin liquids, *npj Quantum Materials* **4**, 12 (2019).
- [19] Y. Li, P. Gegenwart, and A. A. Tsirlin, Spin liquids in geometrically perfect triangular antiferromagnets, *Journal of Physics: Condensed Matter* **32**, 224004 (2020).
- [20] Y. Doi, Y. Hinatsu, and K. Ohoyama, Structural and magnetic properties of pseudo-two-dimensional triangular antiferromagnets Ba₃MSb₂O₉ (M = Mn, Co, and Ni), *J. Phys.: Condens. Matter* **16**, 8923 (2004).
- [21] T. Susuki, N. Kurita, T. Tanaka, H. Nojiri, A. Matsuo, K. Kindo, and H. Tanaka, Magnetization Process and Collective Excitations in the $S=1/2$ Triangular-Lattice Heisenberg Antiferromagnet Ba₃CoSb₂O₉, *Phys. Rev. Lett.* **110**, 267201 (2013).
- [22] G. Koutroulakis, T. Zhou, Y. Kamiya, J. D. Thompson, H. D. Zhou, C. D. Batista, and S. E. Brown, Quantum phase diagram of the $S = \frac{1}{2}$ triangular-lattice antiferromagnet Ba₃CoSb₂O₉, *Phys. Rev. B* **91**, 024410 (2015).
- [23] J. Ma, Y. Kamiya, T. Hong, H. B. Cao, G. Ehlers, W. Tian, C. D. Batista, Z. L. Dun, H. D. Zhou, and M. Matsuda, Static and dynamical properties of the spin-1/2 equilateral triangular-lattice antiferromagnet Ba₃CoSb₂O₉, *Phys. Rev. Lett.* **116**, 087201 (2016).
- [24] Y. Kamiya, L. Ge, T. Hong, Y. Qiu, D. Quintero-Castro, Z. Lu, H. Cao, M. Matsuda, E. S. Choi, C. Batista, M. Mourigal, H. D. Zhou, and J. Ma, The nature of spin excitations in the one-third magnetization plateau phase of Ba₃CoSb₂O₉, *Nature Communications* **9** (2018).
- [25] S. Ito, N. Kurita, H. Tanaka, S. Ohira-Kawamura, K. Nakajima, S. Itoh, K. Kuwahara, and K. Kakurai, Structure of the magnetic excitations in the spin-1/2 triangular-lattice Heisenberg antiferromagnet Ba₃CoSb₂O₉, *Nat. Comm.* **8**, 235 (2017).
- [26] D. Macdougall, S. Williams, D. Prabhakaran, R. I. Bewley, D. J. Voneshen, and R. Coldea, Avoided quasiparticle decay and enhanced excitation continuum in the spin- $\frac{1}{2}$ near-Heisenberg triangular antiferromagnet Ba₃CoSb₂O₉, *Phys. Rev. B* **102**, 064421 (2020).
- [27] R. Chi, Y. Liu, Y. Wan, H.-J. Liao, and T. Xiang, Spin excitation spectra of anisotropic spin-1/2 triangular lattice Heisenberg antiferromagnets, *Phys. Rev. Lett.* **129**, 227201 (2022).
- [28] E. A. Ghioldi, S.-S. Zhang, Y. Kamiya, L. O. Manuel, A. E. Trumper, and C. D. Batista, Evidence of two-spinon bound states in the magnetic spectrum of Ba₃CoSb₂O₉, *Phys. Rev. B* **106**, 064418 (2022).
- [29] E. A. Ghioldi, A. Mezio, L. O. Manuel, R. R. P. Singh, J. Oitmaa, and A. E. Trumper, Magnons and excitation continuum in xxz triangular antiferromagnetic model: Application to Ba₃CoSb₂O₉, *Phys. Rev. B* **91**, 134423 (2015).
- [30] E. A. Ghioldi, M. G. Gonzalez, S.-S. Zhang, Y. Kamiya, L. O. Manuel, A. E. Trumper, and C. D. Batista, Dynamical structure factor of the triangular antiferromagnet: Schwinger boson theory beyond mean field, *Phys. Rev. B* **98**, 184403 (2018).
- [31] A. V. Chubukov, S. Sachdev, and T. Senthil, Quantum phase transitions in frustrated quantum antiferromagnets, *Nuclear Physics B* **426**, 601 (1994).
- [32] R. Coldea, D. A. Tennant, and Z. Tylczynski, Extended scattering continua characteristic of spin fractionalization in the two-dimensional frustrated quantum magnet Cs₂CuCl₄ observed by neutron scattering, *Phys. Rev. B* **68**, 134424 (2003).
- [33] A. O. Scheie, E. A. Ghioldi, J. Xing, J. A. M. Paddison, N. E. Sherman, M. Dupont, L. D. Sanjeewa, S. Lee, A. J. Woods, D. Abernathy, D. M. Pajerowski, T. J. Williams, S.-S. Zhang, L. O. Manuel, A. E. Trumper, C. D. Pemmaraju, A. S. Sefat, D. S. Parker, T. P. Devereaux, R. Movshovich, J. E. Moore, C. D. Batista, and D. A. Tennant, Proximate spin liquid and fractionalization in the triangular antiferromagnet KYbSe₂, *Nature Physics* **20**, 74 (2024).
- [34] L. Chen, D.-W. Qu, H. Li, B.-B. Chen, S.-S. Gong, J. von Delft, A. Weichselbaum, and W. Li, Two-temperature scales in the triangular-lattice Heisenberg antiferromagnet, *Phys. Rev. B* **99**, 140404 (2019).
- [35] P. Prelovsek and J. Kokalj, Finite-temperature properties of the extended Heisenberg model on a triangular lattice, *Phys. Rev. B* **98**, 035107 (2018).
- [36] M. G. Gonzalez, B. Bernu, L. Pierre, and L. Messio, Ground-state and thermodynamic properties of the spin- $\frac{1}{2}$ Heisenberg model on the anisotropic triangular lattice, *SciPost Phys.* **12**, 112 (2022).
- [37] B. Lake, D. A. Tennant, C. D. Frost, and S. E. Nagler, Quantum criticality and universal scaling of a quantum antiferromagnet, *Nature Materials* **4**, 329 (2005).
- [38] M. B. Stone, I. A. Zalitznyak, T. Hong, C. L. Broholm, and D. H. Reich, Quasiparticle breakdown in a quantum spin liquid, *Nature* **440**, 187 (2006).
- [39] A. V. Chubukov and O. A. Starykh, Confinement of spinons in the CP^{M-1} model, *Phys. Rev. B* **52**, 440 (1995).
- [40] D. P. Arovas and A. Auerbach, Functional integral theories of low-dimensional quantum Heisenberg models, *Phys. Rev. B* **38**, 316 (1988).
- [41] A. Auerbach, *Interacting electrons and quantum magnetism* (Springer-Verlag, New York, 1994).
- [42] A. E. Trumper, L. O. Manuel, C. J. Gazza, and H. A. Ceccatto, Schwinger-Boson Approach to Quantum Spin Systems: Gaussian Fluctuations in the “Natural” Gauge, *Phys. Rev. Lett.* **78**, 2216 (1997).
- [43] S.-S. Zhang, E. A. Ghioldi, Y. Kamiya, L. O. Manuel, A. E. Trumper, and C. D. Batista, Large- s limit of the large- n theory for the triangular antiferromagnet, *Phys. Rev. B* **100**, 104431 (2019).
- [44] H. A. Ceccatto, C. J. Gazza, and A. E. Trumper, Non-classical disordered phase in the strong quantum limit of frustrated antiferromagnets, *Phys. Rev. B* **47**, 12329 (1993).
- [45] R. Flint and P. Coleman, Symplectic N and time reversal in frustrated magnetism, *Phys. Rev. B* **79**, 014424 (2009).
- [46] A. Mezio, C. N. Sposetti, L. O. Manuel, and A. E. Trumper, A test of the bosonic spinon theory for the triangular antiferromagnet spectrum, *EPL (Europhysics Letters)* **94**, 47001 (2011).
- [47] P. Azaria, B. Delamotte, and D. Mouhanna, Spontaneous symmetry breaking in quantum frustrated antiferromagnets, *Phys. Rev. Lett.* **70**, 2483 (1993).

- [48] D. Yoshioka and J. Miyazaki, Boson Mean Field Theory of the Triangular Lattice Heisenberg Model, *Journal of the Physical Society of Japan* **60**, 614 (1991).
- [49] T. N. De Silva, M. Ma, and F. C. Zhang, Pathology of Schwinger boson mean-field theory for Heisenberg spin models, *Phys. Rev. B* **66**, 104417 (2002).
- [50] O. Tchernyshyov and S. L. Sondhi, Liquid gas and other unusual thermal phase transitions in some large- N magnets, *Nucl. Phys. B* **639**, 429 (2002), arXiv:cond-mat/0202128.
- [51] J. L. A. Du, G.Z. Wei, Low-temperature properties of the Heisenberg antiferromagnets on the layered triangular lattice, *phys. stat. sol. (b)* **234**, 636 (2002).
- [52] C. Yasuda, S. Todo, K. Hukushima, F. Alet, M. Keller, M. Troyer, and H. Takayama, Néel Temperature of Quasi-Low-Dimensional Heisenberg Antiferromagnets, *Phys. Rev. Lett.* **94**, 217201 (2005).
- [53] L. O. Manuel, A. E. Trumper, and H. A. Ceccatto, Rotational invariance and order-parameter stiffness in frustrated quantum spin systems, *Phys. Rev. B* **57**, 8348 (1998).
- [54] A. Mezio, L. O. Manuel, R. R. P. Singh, and A. E. Trumper, Low temperature properties of the triangular-lattice antiferromagnet: a bosonic spinon theory, *New Journal of Physics* **14**, 123033 (2012).
- [55] M. E. Zhitomirsky and A. L. Chernyshev, *Colloquium* : Spontaneous magnon decays, *Rev. Mod. Phys.* **85**, 219 (2013).
- [56] S. P. Bayrakci, D. A. Tennant, P. Leininger, T. Keller, M. C. R. Gibson, S. D. Wilson, R. J. Birgeneau, and B. Keimer, Lifetimes of antiferromagnetic magnons in two and three dimensions: Experiment, theory, and numerics, *Phys. Rev. Lett.* **111**, 017204 (2013).
- [57] R. Kajimoto, K. Tomiyasu, K. Nakajima, S. Ohira-Kawamura, Y. Inamura, and T. Okuda, Development of Spin Correlations in the Geometrically Frustrated Triangular-Lattice Heisenberg Antiferromagnet CuCrO_2 , *Journal of the Physical Society of Japan* **84**, 074708 (2015).
- [58] J. H. P. Colpa, Diagonalization of the quadratic boson Hamiltonian, *Physica A* **93**, 327 (1978).